Organ of Corti vibrations are dominated by longitudinal motion in vivo

Sebastiaan Meenderink
VA Loma Linda Healthcare System
Wei Dong (wdong@llu.edu)
VA Loma Linda Healthcare System

Article

Keywords: cochlea, gerbil, traveling wave, low-frequency hearing

Posted Date: March 15th, 2022

DOI: https://doi.org/10.21203/rs.3.rs-1405408/v1

Additional Declarations: There is **NO** Competing Interest.

Version of Record: A version of this preprint was published at Communications Biology on November 24th, 2022. See the published version at https://doi.org/10.1038/s42003-022-04234-7.

Organ of Corti vibrations are dominated by longitudinal motion in vivo

Sebastiaan W.F. Meenderink[1], Wei Dong[1–3]

[1] VA Loma Linda Healthcare System, Loma Linda, CA 92374, USA

[2] Department of Otolaryngology – Head and Neck Surgery, Loma Linda University Health, Loma Linda, CA 92350, USA

[3]**corresponding author:** Wei Dong

Email: Wei.Dong[at]va.gov

Competing Interest Statement: The authors declare no competing interests.

Author Contributions: Both authors devised and performed the experiments and wrote the paper. S.M. developed software for data acquisition and analysis.

Keywords: cochlea, gerbil, traveling wave, low-frequency hearing

Abstract

Recent observations of sound-evoked vibrations in the cochlea's sensory organ of Corti (ooC), using optical coherence tomography (OCT), revealed unanticipated and complex motions. Relative motion between different structures of the ooC is the key for mammalian ears to achieve remarkable frequency selectivity and sensitivity but is not well understood, especially in the low-frequency region that is essential to human speech perception. We mapped the ooC motions using multiple OCT viewing angles over an extended region in the low-frequency apex of gerbil cochleae. These resolve the "direction limit" with classical approaches and address low-frequency sound processing in the mammalian ear. Our data demonstrate the active structure of sensory outer hair cells moves with the traveling wave. In addition, they also move along an unexpected longitudinal direction. This motion is never predicted, adds another dimension to address the active process within the cochlea, and impacts the interpretation of cochlear vibrometry data.

Introduction

The mammalian ear processes sound over a wide range of frequencies (e.g., 20–20,000 Hz in humans) and intensities (20 μPa–20 Pa; 120 dB), while maintaining the ability to discriminate tonal frequencies and intensities that differ by only 0.2% and 1 dB, respectively (1). This remarkable performance is achieved predominantly by delicate micromechanical processes in the peripheral inner ear, or cochlea (2). The high sensitivity, wide dynamic range, and frequency selectivity of our hearing all diminish in damaged or postmortem ears (3), but the underlying cochlear mechanics of the living ear are not fully understood. The cochlea is an elongated and spiraled conical structure (Fig. 1A) that is part of the bony labyrinth, located in the skull's temporal bone. It is partitioned into two fluid-filled tubes by the stiff BM that supports the ooC. Sound, entering near the cochlea's base via the stapes, evokes a traveling wave (TW) that propagates in the longitudinal direction towards the apex. Systematic changes in several anatomical and biophysical properties along the cochlear length affect the local amplitude and propagation speed of the TW and its dependence on frequency (4). This creates a place-based spectral decomposition of sound, or tonotopic organization, in which high frequencies maximally excite the cochlear base and low frequencies the apex. During TW propagation, the active outer hair cell (OHC) responses play a pre-eminent role in maintaining normal hearing, but our understanding of the underlying mechanisms is incomplete. More detailed information of sound-evoked vibrations along the BM and from key structures within the ooC is needed to determine how the cochlear micromechanics contribute to our exquisite sense of hearing.

Unfortunately, the internal cochlear structures are small and poorly accessible. Moreover, their responses are on a (sub-)nanometer scale and vulnerable to physiological insult (3). This makes measuring in vivo vibrations extremely difficult, and until recently they were only recorded from superficial structures (e.g., BM) at a few longitudinal locations. Spectral-domain OCT overcomes several of these limitations and facilitates vibration measurements from structures within the ooC (5, 6) that revealed several unanticipated and complex motions (7–12). Although only separated from the BM by 20–100 μm, OHC-responses differed substantially and were more complex than the BM response: they had larger amplitudes and different phases, displayed wideband (hyper-)compression, and exhibited more rectification and distortion products. The interpretation of these observations is, however, frustrated by the measurement technique in that it only measures the component of the displacement that is projected onto the system's optical path. This methodological limitation is severe when interpreting vibrations within the ooC. While BM vibrations are largely restricted to the cross-sectional plane (4), ooC structures can also move in the longitudinal direction, in-and-out of this plane. Such motion has only been observed in excised cochleae (13), with indirect evidence in recent in vivo experiments (7). Without knowing the motion directions, any interpretation of the observed complex motion patterns becomes tentative.

Measured amplitude differences may reflect differences in motion direction rather than in true amplitude along the OCT optical path, and the same holds for the phase. More concretely, data from two points (e.g., the two ends of an OHC) may be interpreted either in terms of length changes or as a rotation of the structure. Without knowing the vibration directions, it is impossible to decide between the two.

Direction of motion can be determined by measuring responses at different angles between the OCT optical path and the vibrating structure. One method to vary this "viewing angle" is to rotate the OCT's beam direction relative to the inner ear (12), but anatomical restrictions due to the cochlea's location make this difficult. The curved nature of the cochlear partition, however, offers a unique alternative to systematically vary the viewing angle in small steps without having to move the preparation or rotate the OCT (Fig. 1, see also Fig. 4D). Exploiting this curvature, we recorded BM and OHC vibrations at adjacent locations with a gradually changing viewing angle. At near-perpendicular angles between the beam and the longitudinal axis of the ooC, we consistently observed an abrupt 180-degree phase flip in the vibrations of the OHCs. This abrupt polarity reversal is evidence that OHC displacements were largest in the longitudinal direction such that they dominated the measured response for most of the viewing angles. Effectively, the projection of any radial or transverse OHC vibrations was "masked" by longitudinal motion in the measured response. This finding warrants a re-evaluation of all cochlear vibrometry data in the literature: large longitudinal displacements occur in vivo, and their effect must be accounted for prior to attributing significance to any observed motions within the ooC.

Results

With our OCT system we visualized a 0.6–0.8 mm stretch along the longitudinal axis of the second-turn gerbil cochlea (Fig. 1A, B). Across this section the cochlea coiled appreciably, resulting in considerable variation in the OCT viewing angle relative to the longitudinal axis of the BM (between -23^{o} and $+19^{o}$ across animals; Fig 1B, inset). At multiple locations along this axis, orthogonal (cross-sectional) images were obtained (Fig. 1C) in which sound-evoked vibrations of the BM and the OHC were recorded from two representative locations (8, 11, 12, 14). These locations were chosen such that, across tonotopic locations, the distance between the BM and OHC did not change ($F_{1,37}$=1.63, p=0.21; mean distance: 91.5 μm).

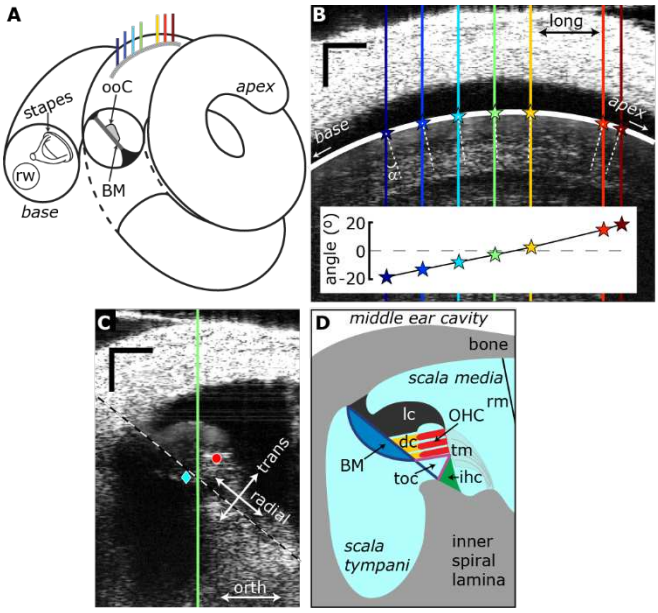

Figure 1. Different viewing angles in the 2nd turn of the cochlea. (**A**) Schematic diagram of the spiral gerbil cochlea with a cross-sectional plane (orthogonal to the longitudinal axis) in the 2nd turn exposed to show the basilar membrane (BM) and the organ of Corti (ooC). The gray line with colored lines represents the image location shown in (B). Colored lines indicate beam positions used for vibrometry. (**B**) Intensity image along the longitudinal axis in the 2nd turn of the gerbil cochlea. Solid white line: ellipse fitted to the boundary of the lateral compartment of the ooC, serving to determine the viewing angle (see Methods). Inset: viewing angles of the beams (colored lines). Scale bars, 0.1 mm. (**C**) Example cross-sectional intensity image, orthogonal to the longitudinal axis, obtained at the location indicated by the green line in (B). The cyan diamond (BM) and red circle (OHC region) indicate locations at which sound-evoked vibrations were recorded. The green line locates the intersection with the longitudinal plane, the dashed black/white line indicates the BM. View into the paper is along the longitudinal axis, towards cochlear apex. Scale bars, 0.1 mm. (**D**) Schematic of the anatomical structures for the cross section shown in (C). Fluid-filled spaces within the cochlea are light blue. BM: basilar membrane, dc: Deiter's cells, ihc: inner hair cell region, lc: lateral compartment, OHC: outer hair cell region, ooC: organ of Corti, orth: orthogonal, toc: tunnel of Corti, trans: transverse, rm: Reissner's membrane, rw: round window, tm: tectorial membrane.

BM frequency response curves (FTC) were tuned (Fig. 2A) to best frequencies (BFs) that systematically decreased from 2.8 kHz to 2.0 kHz at the most basal and apical locations, respectively, in agreement with the tonotopic organization of the cochlea (Fig. 2F; diamonds). Using a cochlear place-frequency map obtained from gerbil auditory nerve fibers (15), these BFs indicated that the recording locations were between 6.5 and 7.3 mm from the base of the cochlea. For each BM-FTC, the phase (Fig. 2C) accumulated with frequency in a manner characteristic for a longitudinally propagating TW that slowed down when approaching the location's BF. We calculated wavelengths (λ) from BM phase responses across the tonotopic recording locations (Fig. 2G) and found them to vary with frequency between $\lambda \approx$ 1 mm near BF and $\lambda \approx$ 2–3.5 mm below BF. These values are similar to wavelength estimates in the ~3-kHz region from cochlear-mechanical (3, 16, 17) and auditory-nerve data (18). Like the BM responses, OHC-FTCs were tuned (Fig. 2B) with similar BFs that decreased with tonotopic location (Fig. 2F;

circles), although they exhibited a substantially larger sub-BF response (7, 11). The accompanying phase curves (Fig. 2D) also showed location-dependent TW characteristics, but they differed from the BM phase data in that these curves were arranged in two groups that differed by ~0.5-cycle in their vertical offset. As a result, OHC responses either lagged or lead the BM by ~0.25 cycle (Fig. 2E). The dramatic character of the phase reversal of OHC motion is illustrated by plotting the OHC–BM phase difference as a function of viewing angle (Fig. 3A). The phase difference exhibited a robust trend: for negative viewing angles, corresponding to the higher-CF tonotopic locations, the OHC responses led the BM by ~0.25 cycles, which abruptly transitioned to a quarter-cycle phase lag when the viewing angles were positive.

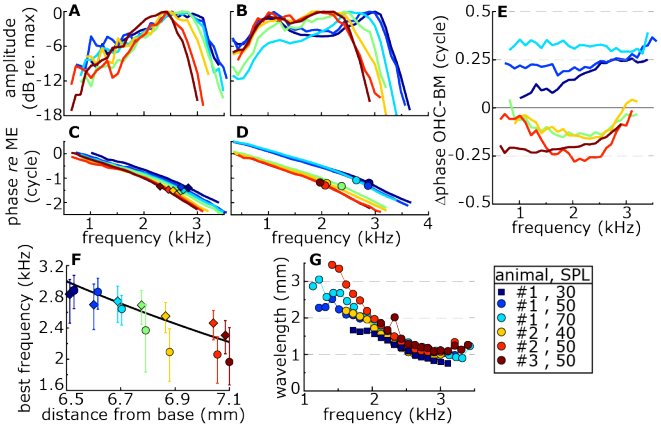

Figure 2. Vibratory responses along the tonotopic axis of the cochlea. Amplitude of (**A**) BM and (**B**) OHC vibratory frequency response curves (FTCs) measured at different longitudinal locations in the gerbil cochlea. Different colors correspond to the color coding for recording location in Fig. 1B. (**C, D**) Corresponding phase data, normalized to the middle-ear (ME) response. Diamonds and circles indicate best frequency (BF). (**E**) Phase difference between the responses in the OHC region and on the BM at each longitudinal recording location. (**F**) BF for the BM (diamonds) and the OHC region (circles) determined from the FTC amplitude curves. Error bars give FTC-bandwidth at 1-dB below the BF response. The black line is a fit of the gerbil place-frequency map (15) to the BM-BFs. This fit was used to set the values along the abscissa. Stimulus level: 30 dB SPL per frequency component. (**G**) Wavelength of the TW. Here, each color represents a separate set of recordings that was obtained across different longitudinal locations (see legend): the square, darkest-blue symbols are from the phase data in C.

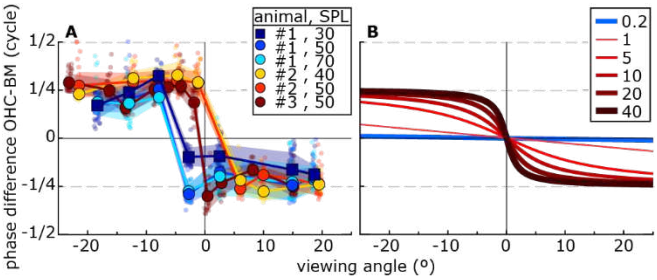

Figure 3. Viewing angle determines the phase difference between OHC and BM. (**A**) The six curves show OHC–BM phase difference, averaged across frequency, as a function of viewing angle α relative to the longitudinal axis of the BM (see Fig. 1B) for different series of recordings. These were from n=3 gerbils at several sound pressure levels (see legend). Small colored circles give individual data points, shaded areas show ± 1 s.d. around the mean. The square, darkest-blue symbols are for the recordings in Figs. 1,2. (**B**) Expected phase differences for elliptical motion (see text) with different aspect ratio, here, amplitude ratio of

longitudinal and the orthogonal vibrations (see legend). For ratios>1 (i.e., a larger longitudinal component, red lines), the phase difference systematically varies between +0.25 and –0.25 cycles. The 0.5-cycle transition occurs more abruptly for larger amplitude ratios. When the orthogonal motion is larger (ratio<1, blue line), only a small phase difference occurs for these viewing angles. Irrespective of amplitude ratio, the phase difference flips sign when α=0°.

Discussion

The data presented here reveal a phase difference between the BM and OHC vibratory responses that strongly depended on the angle between the BM along the longitudinal axis of the cochlea and the incident OCT light beam. As discussed below, we interpret this result to indicate that sound-evoked OHC motions are primarily along the tonotopic axis, which effectively masks contributions from any OHC motion in the radial and/or transverse directions. Since viewing angle and cochlear tonotopic location co-vary in these experiments, either can potentially underlie the observed effect. However, it is very unlikely that local changes in the anatomy or physiology would underlie the phase reversals: (1) the reversal is complete between points separated by only ~100 μm along the cochlear length; (2) over the same spatial range the changes in BM vibration are small and gradual (Fig. 2C); (3) the same reversal was observed in all animals, despite differences in anatomy and experimental conditions; (4) the reversals would require a sudden change in the local anatomical and/or electro-mechanical ooC properties, which is not observed (19–22). Rather, the observed phase reversal can readily be explained by considering displacements in the longitudinal direction that lag the transverse vibrations by 0.25 cycle, a scenario encountered in many types of waves (23). OCT measures the projection of the actual motion onto its optical beam. When the actual motion contains both longitudinal and non-longitudinal components, their relative contribution to the measurement depends on their relative magnitudes and the OCT viewing angle. A simple geometric relation (7) describes how the OHC–BM phase difference depends on both viewing angle and the relative vibration size (Fig. 3B). Accepting a few degrees of uncertainty in determining the viewing angles, the data (Fig. 3A) are qualitatively and quantitatively well described by the situation in which longitudinal motion dominates the recorded OHC vibrations, thus masking any contributions from motion within the cross-sectional (transverse-radial) plane to the measured response. Although a description of the cochlea is undoubtedly more complex due to the presence of the ooC with its internal (anisotropic) structures, it is informative to consider the hydrodynamics of familiar waves on water, i.e., traveling waves on the surface of a homogeneous fluid layer plane ((23–25) see also Fig. 4A–C).

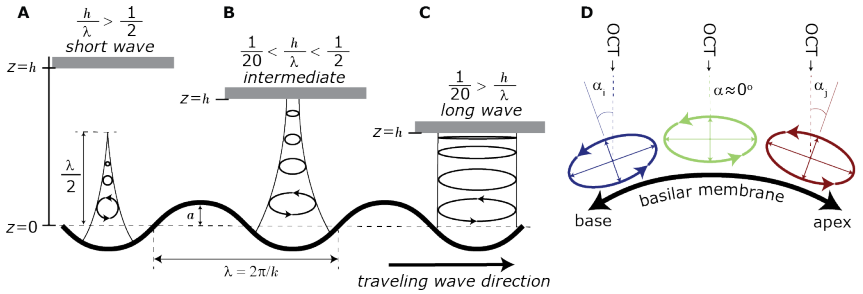

Figure 4. Elliptical particle motion associated with a surface wave. (A–C) A surface wave that travels from left to right (thick black line) is associated with elliptical trajectories of fluid particles. For each cycle of the TW this ellipse is traversed once in the counterclockwise direction. The shape of these ellipses depends on the depth of the wave medium (*h*) relative to the TW wavelength (λ), and three *h*/λ-regimes are recognized (26): (**A**) short wave (deep water), (**B**) intermediate, and (**C**) long wave (shallow water). For short waves (**A**), *h* has no effect, and the amplitudes of the longitudinal and transverse motions are identical, resulting in circular motion. The sizes of these circles decay exponentially with depth into the wave medium, and at *z*=λ/2 are less than 5% of the TW amplitude *a*. In contrast, for long waves (**C**) the ellipses are substantially flattened in the transverse direction (i.e., longitudinal motion is at least 10 dB larger than transverse motion). Moreover, the amplitude of the longitudinal motion decays little with distance away from TW-supporting surface, while the transverse amplitude reduces linearly with depth. (**D**) Due to the natural curvature of the cochlea/BM in the longitudinal direction (thick black line), a vertical OCT measurement beam (dashed lines) will view the elliptical motion at an angle (α) that varies with tonotopic location within the cochlea (different colors). We used this to show that the measured phase difference between the BM and OHC responses was caused by projection of longitudinal motion onto the measurement beam.

In general, conservation of volume makes that transverse surface displacements move fluid particles in both the longitudinal and orthogonal direction, where the former lags the latter by 0.25 cycle. This also applies to the more complex cochlear situation; the fluid within cannot be compressed. As a result, fluid particles move in a counterclockwise direction along ellipses that are oriented parallel to the propagation direction of the TW. These ellipses vary from circular (Fig. 4A) to extremely flattened in the longitudinal direction (Fig. 4C) depending on the wavelength of the TW relative to the depth of the fluid. The rapid transition in the observed phase differences (Fig. 3A) suggests that the ellipses are relatively flat, and that the cochlea thus operates in the long-wave regime in which the TW wavelength is at least 20× larger than the effective depth of the wave medium (26). Wavelengths of 1–3 mm (Fig. 2G) correspond to an effective cochlear fluid depth of at most 50–175 μm. This is on the same order as the ooC dimensions, suggesting that perhaps the tectorial membrane or reticular lamina served as the fixed "wall" rather than the bony walls of the osseous labyrinth.

Irrespective of their origin, the data show longitudinal vibrations within the OHC region of the ooC that far exceeded the amplitudes of vibrations in the cross-sectional plane. Although this makes any interpretation of the complex motions observed within the ooC in terms of (relative) transverse or radial vibrations speculative, it may explain why, from all the different intracochlear vibrations that have been documented, BM responses are most like the tuned auditory nerve fiber (ANF) response (27, 28). It would

not be surprising that when the longitudinal responses are quantified and accounted for, the apparent complexity of intra-ooC vibrations is much reduced such that they become more like the well-known BM and ANF responses.

Materials and Methods

Animal preparation. The care and use of animals were in accordance with guidelines of, and approved by, the Institutional Animal Care and Use Committee (IACUC) of the VA Loma Linda Healthcare System. Cochlear vibrations were measured from the left ear in adult, female Mongolian gerbils (*M. unguiculatus*, *n*=3) that were part of a larger study group. Animals were anesthetized using intraperitoneal injections of a ketamine/xylazine (80 and 10 mg/kg, respectively) cocktail. Supplemental doses were administered to maintain areflexia. Core temperature was kept at ~38 ^{o}C using a heating pad (Harvard Apparatus). Animals were tracheotomized, but not actively ventilated. A ventrolateral surgical approach exposed the left bulla, which was opened to visualize the cochlea. The pinna and the cartilaginous ear canal were resected, and a probe containing a microphone and transducer assembly (ER-10X, Etymotic Research) was placed within a few mm of the tympanic membrane. Animals were not allowed to recover from anesthesia and were euthanized by anesthetic overdose at the end of the experiment.

Optical coherence tomography and vibrometry. A spectral domain OCT system (Thorlabs Telesto III TEL321C1 equipped with an LSM04 objective) that operated with a central wavelength of 1310 nm (bandwidth: 170 nm) was used to noninvasively image through the cochlear bone and record the vibratory responses in the middle turn of the exposed, but otherwise structurally uncompromised, cochlea. Acquisition of optical spectra was controlled by externally generated TTL pulses (rate: 27.9 pulses/ms) that were synchronized to the stimulus generation and microphone acquisition system (RX6: Tucker Davies Technologies system III). These spectra were converted into depth-resolved, axial information (A-line) using Fourier analysis. Intensity images (B-scans) were constructed from multiple A-lines by scanning the OCT either along the longitudinal axis of the cochlea (Fig. 1B), or in a perpendicular direction to obtain cross-sectional images through the cochlear duct (Fig. 1C). To improve the quality of these images, the scan path was traversed multiple (>10) times and the intensity profiles averaged. For vibration measurements (M-scans), the axial phase information of the A-lines was used. Here, the OCT measurement beam was kept at a fixed position, and a series of time-stamped A-lines was recorded while an acoustic stimulus was presented to the ear. Between M-scans, the angle between the vertical OCT beam and the organ of Corti varied due to the natural curvature of the cochlea (Fig. 4D), which allowed us to assess the relative size of vibrations in the longitudinal and cross-sectional plane. Vibratory responses of the umbo were recorded immediately following each animals' death and served as a reference for the phase of the intracochlear responses.

Acoustic stimulation and analysis. Acoustic stimuli consisted of 42 equal-intensity frequency components, each one with a random starting phase. Sound pressure levels were calibrated *in situ* and are expressed in decibels re. 20 μPa (i.e., dB SPL). Stimulus frequencies were irregularly spaced ("zwuis": see (29)) and were chosen such that they all had a whole number of cycles over a "periodic block" of w=334,821 samples (~12 s). Typically, 3–5 concatenated periodic stimulus blocks were presented (i.e., stimulus duration: 36–60 s). The stimulus was preceded and followed by a ~100-ms signal to accommodate ramps (5 ms, raised cosine) that turned on and off the tone complex, respectively. The average response waveform across the periodic blocks was calculated (ignoring the 100-ms onset and offset) from which the responses at the stimulus frequencies were extracted using Fourier analysis. No artifact rejection was employed. A frequency component was considered above noise when a Rayleigh's test for uniformity indicated significant (p≤0.001) phase locking to the stimulus (30).

In each longitudinal OCT image, a tilted ellipse was fitted to the boundary of the lateral compartment of the ooC (Fig. 1B). The angle between the normal of this ellipse and the vertical OCT beam was calculated at the longitudinal locations at which cross-sectional OCT images were obtained (Fig 1B; inset). These angles served as an estimate for the angle between the OCT beam and the BM in the longitudinal direction (termed "viewing angle α" in the manuscript).

Frequency-dependent wavelength (Fig. 2G) was calculated by fitting a straight line to the phase-vs-position data at each stimulus frequency using least-square minimization. The estimate was excluded when r^2<0.8. Custom software for stimulus generation, synchronization, and all signal analysis (including statistics and regression) was implemented in Matlab; control of the OCT system was programmed in C#.

Acknowledgments

We thank Drs. Peter Narins, Hyle Park and Xiaohui Lin. This work was supported by NIH/NIDCD R01DC011506, R21DC019998, and VA Merit Award C2296-R to W.D.

Data availability

All data presented in this study (Figs. 1–3) are available for download at figshare (https://doi.org/10.6084/m9.figshare.18217127.v1).

References

1. W. A. Yost, *Fundamentals of Hearing: an introduction*, 2nd Ed. (Holt Rinehart and Winston, 1985).
2. N. B. Slepecky, "Structure of the mammalian cochlea" in *The Cochlea*, P. Dallos, A. N. Popper, R. R. Fay, Eds. (Springer, 1996), pp. 44–129.
3. L. Robles, M. A. Ruggero, Mechanics of the mammalian cochlea. *Physiol. Rev.* **81**, 1305–1352 (2001).

4. G. von Békésy, *Experiments in Hearing* (McGraw-Hill, 1960).

5. N. Choudhury, *et al.*, Low coherence interferometry of the cochlear partition. *Hear. Res.* **220**, 1–9 (2006).

6. R. K. Wang, A. L. Nuttall, Phase-sensitive optical coherence tomography imaging of the tissue motion within the organ of Corti at a subnanometer scale: a preliminary study. *J. Biomed. Opt.* **15**, 056005 (2010).

7. N. P. Cooper, A. Vavakou, M. van der Heijden, Vibration hotspots reveal longitudinal funneling of sound-evoked motion in the mammalian cochlea. *Nat. Commun.* **9** (2018).

8. J. B. Dewey, B. E. Applegate, J. S. Oghalai, Amplification and suppression of traveling waves along the mouse organ of Corti: evidence for spatial variation in the longitudinal coupling of outer hair cell-generated forces. *J. Neurosci.* **39**, 1805–1816 (2019).

9. J. B. Dewey, A. Altoè, C. A. Shera, B. E. Applegate, J. S. Oghalai, Cochlear outer hair cell electromotility enhances organ of Corti motion on a cycle-by-cycle basis at high frequencies in vivo. *Proc. Natl. Acad. Sci.* **118**, e2025206118 (2021).

10. W. He, T. Ren, The origin of mechanical harmonic distortion within the organ of Corti in living gerbil cochleae. *Commun. Biol.* **4** (2021).

11. T. Ren, W. He, D. Kemp, Reticular lamina and basilar membrane vibrations in living mouse cochleae. *Proc. Natl. Acad. Sci.* **113**, 9910–9915 (2016).

12. H. Y. Lee, *et al.*, Two-dimensional cochlear micromechanics measured in vivo demonstrate radial tuning within the mouse organ of Corti. *J. Neurosci.* **36**, 8160–8173 (2016).

13. K. D. Karavitaki, D. C. Mountain, Imaging electrically evoked micromechanical motion within the organ of Corti of the excised gerbil cochlea. *Biophys. J.* **92** (2007).

14. W. He, D. Kemp, T. Ren, Timing of the reticular lamina and basilar membrane vibration in living gerbil cochleae. *eLife* **7** (2018).

15. M. Müller, The cochlear place-frequency map of the adult and developing Mongolian gerbil. *Hear. Res.* **94** (1996).

16. O. de La Rochefoucauld, E. S. Olson, The role of organ of Corti mass in passive cochlear tuning. *Biophys. J.* **93**, 3434–3450 (2007).

17. W. S. Rhode, A. Recio, Study of mechanical motions in the basal region of the chinchilla cochlea. *J. Acoust. Soc. Am.* **107**, 3317–3332 (2000).

18. M. van der Heijden, P. X. Joris, Panoramic measurements of the apex of the cochlea. *J. Neurosci.* **26**, 11462–11473 (2006).

19. G. Emadi, C.-P. Richter, P. Dallos, Stiffness of the gerbil basilar membrane: radial and longitudinal variations. *J. Neurophysiol.* **91**, 474–488 (2004).

20. S. W. F. Meenderink, C. A. Shera, M. D. Valero, M. C. Liberman, C. Abdala, Morphological immaturity of the neonatal organ of Corti and associated structures in humans. *J. Assoc. Res. Otolaryngol.* **20**, 461–474 (2019).

21. R. Pujol, M. Lenoir, S. Ladrech, F. Tribillac, G. Rebillard, “Correlation between the length of outer hair cells and the frequency coding of the cochlea” in *Auditory Physiology and Perception*, (Elsevier, 1992), pp. 45–52.

22. D. E. Zetes, J. A. Tolomeo, M. C. Holley, Structure and mechanics of supporting cells in the guinea pig organ of Corti. *PLoS ONE* **7**, e49338 (2012).

23. M. W. Dingemans, *Water wave propagation over uneven bottoms, part 1. Linear wave propagation* (World Scientific, 1997).

24. J. Lighthill, *Waves in Fluids* (Cambridge University Press, 1978).

25. J. Lighthill, Energy flow in the cochlea. *Journal of Fluid Mechanics* **106**, 149–213 (1981).

26. R. G. Dean, R. A. Dalrymple, *Water Wave Mechanics for Engineers and Scientists* (World Scientific, 1991).

27. S. S. Narayan, A. N. Temchin, A. Recio, M. A. Ruggero, Frequency tuning of basilar membrane and auditory nerve fibers in the same cochleae. *Science* **282**, 1882–1884 (1998).

28. M. A. Ruggero, S. S. Narayan, A. N. Temchin, A. Recio, Mechanical bases of frequency tuning and neural excitation at the base of the cochlea: comparison of basilar-membrane vibrations and auditory-nerve-fiber responses in chinchilla. *Proc. Natl. Acad. Sci.* **97**, 11744–11750 (2000).

29. S. W. F. Meenderink, M. van der Heijden, Reverse cochlear propagation in the intact cochlea of the gerbil: evidence for slow traveling waves. *J. Neurophysiol.* **103**, 1448–1455 (2010).

30. C. P. C. Versteegh, M. van der Heijden, Basilar membrane responses to tones and tone complexes: nonlinear effects of stimulus intensity. *J. Assoc. Res. Otolaryngol.* **13**, 785–798 (2012).